

# Electrocatalytic H<sub>2</sub> evolution promoted by a bioinspired (N<sub>2</sub>S<sub>2</sub>)Ni(II) complex at low acid concentration

Soumalya Sinha,<sup>[a],#</sup> Giang N. Tran,<sup>[a],#</sup> Hanah Na,<sup>[a]</sup> and Liviu M. Mirica\*<sup>[a]</sup>

[a] Dr. S. Sinha, G. N. Tran, Dr. H. Na, Prof. L. M. Mirica  
Department of Chemistry  
University of Illinois at Urbana Champaign  
600 S. Mathews Avenue, Urbana, Illinois 61801  
\* E-mail: [mirica@illinois.edu](mailto:mirica@illinois.edu)

[#] These authors contributed equally

Supporting information for this article is given via a link at the end of the document.

**Abstract:** The electrochemical hydrogen evolution reaction (HER) is of great interest to advance fuel cell technologies. Although heterogeneous HER electrocatalysts are desired for practical energy devices, the development of molecular electrocatalysts is important to elucidate the mechanism and improve the activity of state-of-the-art HER catalysts. Inspired by the enzymatic HER process promoted by [NiFe] hydrogenases, we synthesized a bioinspired Ni<sup>II</sup> electrocatalyst that produces H<sub>2</sub> from CF<sub>3</sub>CO<sub>2</sub>H at low acid concentrations (<0.043 M) in MeCN. Under these conditions, the turnover frequency for HER achieved herein is ~200,000 s<sup>-1</sup>. We propose that our Ni<sup>II</sup> electrocatalyst follows a novel HER mechanism by undergoing a 2e<sup>-</sup> transfer process in a single step, followed by stepwise H<sup>+</sup> transfer at low acid concentrations, and the increase in acid concentration changes the HER mechanism toward a concerted H<sup>+</sup>/e<sup>-</sup> transfer. Finally, we evaluated the HER activity of our catalyst by benchmarking its kinetic and thermodynamic parameters vs. other reported HER electrocatalysts.

Hydrogen (H<sub>2</sub>) is a key ingredient for fuel cell technologies needed for the future use of renewable energy sources on a larger scale.<sup>1</sup> The primary challenge of such technologies is to implement earth-abundant materials to produce H<sub>2</sub> with high turnover frequency (TOF) using mild acids. In this area, biological catalysts such as [NiFe] hydrogenases have been the inspiration for reducing H<sup>+</sup> to H<sub>2</sub>, with TOF of ~1000 sec<sup>-1</sup> under weak acidic conditions.<sup>2-3</sup> This enzymatic H<sub>2</sub> evolution reaction (HER) employs only first-row transition metals, Fe and Ni, to perform the 2e<sup>-</sup> reduction process.<sup>4</sup> Additionally, the H<sup>+</sup> transfer events are controlled at the Ni center, which is ligated two terminal cysteine (Cys) groups and two bridging Cys thiolates. The final intermediate in such an enzymatic HER cycle is the Ni-R state that releases H<sub>2</sub> and returns to the resting state, Ni-S<sub>1</sub>a (Figure 1).<sup>5-6</sup>

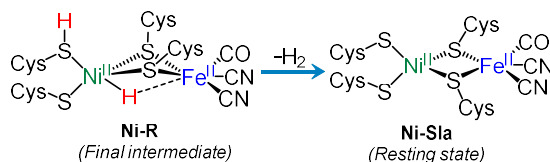


**Figure 1.** The final step observed in [NiFe] hydrogenases catalyzed HER cycle.

Although structural mimics of [NiFe] hydrogenases have been explored, their performance in catalytic HER is either not described or kinetically sluggish.<sup>7-11</sup> Furthermore, there are other efficient mononuclear Ni complexes reported for electrocatalytic HER. For example, DuBois and co-workers reported Ni

phosphine complexes that feature flexible amine arms as proton relay groups and perform HER using a strong acid, protonated dimethylformamide ([DMF-H]<sup>+</sup>, pK<sub>a</sub> = 6.1 in MeCN).<sup>12-13</sup> Dempsey and co-workers investigated the electrochemical HER mechanism of such Ni phosphine complexes and showed that the flexible second coordination sphere amine arms do not coordinate with the Ni center, yet they only shuttle protons through H-bonding.<sup>14</sup> Therefore, we consider that such amine proton relay groups do not faithfully resemble the Cys groups in [NiFe] hydrogenases.

A few reported molecular Ni<sup>II</sup> electrocatalysts perform HER at low overpotential using weak acids. Jones and co-workers reported a mixed thiolate/phosphine S<sub>2</sub>P<sub>2</sub>-coordinated Ni HER electrocatalyst, which produces H<sub>2</sub> from CH<sub>3</sub>CO<sub>2</sub>H (AcOH, pK<sub>a</sub> = 22.48 in THF) at only 240 mV of overpotential, yet with a low TOF of 1240 s<sup>-1</sup>.<sup>15</sup> Furthermore, a Ni complex bearing phosphinopyridyl ligands with amine residues as H<sup>+</sup> transfer sites showed comparatively higher TOF of 8400 s<sup>-1</sup> using AcOH in MeCN (pK<sub>a</sub> = 23.51), but at a high overpotential (590 mV).<sup>16</sup>

Herein we report the synthesis and characterization of a bioinspired Ni complex [(N<sub>2</sub>S<sub>2</sub>)Ni<sup>II</sup>(MeCN)<sub>2</sub>](OTf)<sub>2</sub>, **1**•(OTf)<sub>2</sub>, where N<sub>2</sub>S<sub>2</sub> is 3,7-dithia-1,5(2,6)-dipyridinacyclooctaphane (Figure 2). We then studied the electrocatalytic HER reactivity of **1**<sup>2+</sup> in MeCN using the acids CF<sub>3</sub>CO<sub>2</sub>H (TFA, pK<sub>a</sub> = 12.65)<sup>17</sup> or AcOH as the proton sources. Importantly, we evaluated the HER performance of **1**<sup>2+</sup> using low acid concentrations, ≤0.043 M for TFA and ≤0.058 M for AcOH, respectively, in wet MeCN. Remarkably, **1**<sup>2+</sup> showed a fast HER electrocatalytic activity with a maximum TOF of 195,000 s<sup>-1</sup> using only 0.043 M of TFA in MeCN with ≤2 M H<sub>2</sub>O. We attribute such elevated performance of **1**<sup>2+</sup> to the participation of the pyridyl group of the N<sub>2</sub>S<sub>2</sub> ligand in proton binding and transfer events during HER, and thus mimicking the role of Cys residues in [NiFe] hydrogenases.

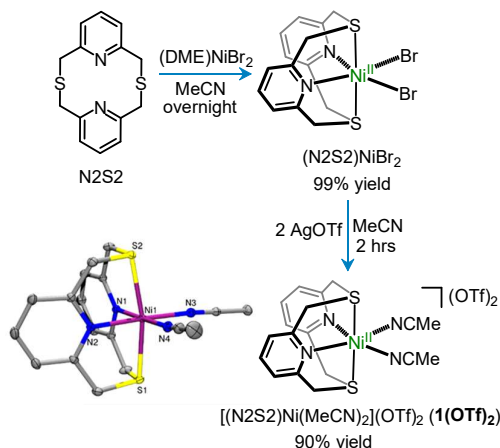


**Figure 2.** Synthetic scheme for  $[(N_2S_2)Ni(MeCN)_2](OTf)_2$  ( $1\bullet(OTf)_2$ ) and ORTEP representation (50% probability ellipsoids) for  $1^{2+}$  (bottom left). Selected bond distances (Å): Ni1–N1 2.071(9), Ni1–N2 2.060(10), Ni1–S1 2.379(3), Ni1–S2 2.394(3), Ni1–N3 2.060(10), Ni1–N4 2.039(10).

The  $N_2S_2$  ligand was prepared following a slightly modified literature procedure<sup>18</sup> and obtained as a white solid with 56% yield.<sup>19</sup> The synthesis of  $1\bullet(OTf)_2$  was then optimized in two steps (Figure 2) and one-step synthetic routes,<sup>19</sup> and obtained as a purple solid with 90% and 82% yield, respectively. The X-ray crystallography data of  $1\bullet(OTf)_2$  reveals a distorted octahedral coordination of the  $Ni^{II}$  center, with the two N atoms of the  $N_2S_2$  ligand and two MeCN molecules occupying the equatorial positions, with an average Ni–N bond distance of 2.06 Å (Figure 2). The two S atoms of  $N_2S_2$  occupy the axial positions with comparatively longer average Ni–S bond lengths of 2.386 Å, thus completing a  $\kappa^4$  binding mode for the  $N_2S_2$  ligand.

We then studied the electrochemical behavior of  $1^{2+}$  in  $N_2$ -saturated 0.1 M  $nBu_4NPF_6$  (TBAP)/MeCN solution, and all redox potentials reported herein are referenced vs. the ferrocenium-ferrocene couple ( $Fc^{+/0}$ ).<sup>19</sup> The cyclic voltammograms (CVs) of  $1^{2+}$  showed a quasi-reversible redox wave centered at  $-1.30$  V and an irreversible wave at  $-1.75$  V, assigned to the  $Ni^{III}/Ni^{II}$  and  $Ni^{II}/Ni^0$  redox couples, respectively (Figure 3a). Scan rate dependence CVs confirmed diffusion-controlled electrochemical processes by exhibiting a linear correlation between the cathodic peak currents at the  $Ni^{III}/Ni^{II}$  redox wave and the square root of the scan rates (Figure 3b).<sup>20</sup>

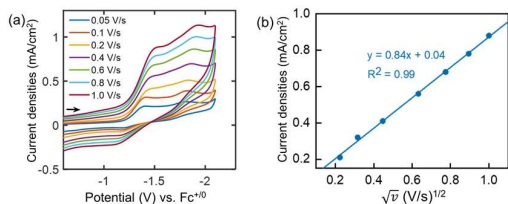


**Figure 3.** (a) CVs of  $1^{2+}$  in  $N_2$ -saturated 0.1 M TBAP/MeCN solution at different scan rates (0.1 – 1.0 V/s). (b) Peak current densities obtained at the  $Ni^{III}/Ni^{II}$  reductive wave from (a) are plotted vs. the square root of the scan rates ( $\sqrt{v}$ ).

The electrochemical HER activity of  $1^{2+}$  was first tested using AcOH in MeCN. The addition of AcOH showed an increase in the peak current densities at potentials lower than  $-2$  V (Figure S7), yet the current enhancement for  $1^{2+}$  overlapped with the blank electrode contribution (Figure S11). A stronger acid, TFA, was then chosen, and its activity in the absence of  $1^{2+}$  was

benchmarked. Two reductive waves were observed for TFA using a glassy carbon (GC) working electrode (Figure S1), as expected for a strong acid in MeCN.<sup>17</sup>

The CVs recorded for  $1^{2+}$  exhibited catalytic current enhancement in the presence of TFA in MeCN, and the peak currents increased as the concentration of TFA was increased systematically up to  $\sim 70$  mM (Figure 4). The onset potentials of these catalytic CVs were at least 500 mV more positive than the reduction potential of  $Ni^{III}/Ni^{II}$ ,  $E_{Ni(III/II)}$ . Additionally, the catalytic peak potentials ( $E_{cat}$ ) were  $\geq 365$  mV more positive than that of GC-promoted HER in the absence of  $1^{2+}$  (Figure S12).

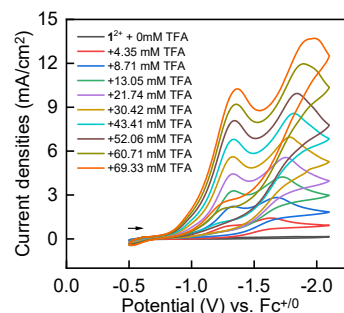


**Figure 4.** CVs of  $1^{2+}$  (1 mM) without (black) and with different concentrations of TFA (4.35 mM – 69.33 mM) in  $N_2$ -saturated 0.1 M TBAP/MeCN. Scan rate = 0.1 V/s.

The mechanism of HER process catalyzed by  $1^{2+}$  was then investigated. The shift in  $E_{Ni(III/II)}$  was first plotted vs. the logarithm of TFA concentration and fitted linearly (Figure 5a). At lower TFA concentrations,  $< 0.043$  M, the slope of such linear fit is 23 mV/dec (Figure 5a, blue dots), indicating a  $2e^-$  transfer step followed by a rate-limiting proton transfer process.<sup>20</sup> Interestingly, the slope value changed to 179 mV/dec at higher TFA concentration ( $> 0.043$  M, Figure 5a, red dots) and that could be attributed as a rate-limiting concerted proton-coupled electron transfer (CPET) step at high proton concentration.<sup>20</sup>

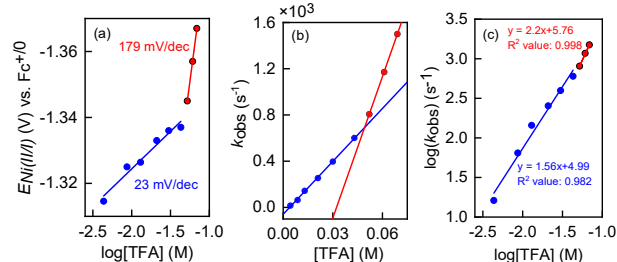


**Figure 5.** (a) Plot of  $Ni^{III}$  reduction potential vs. logarithm of [TFA], 4.35 – 43.41 mM (blue dots) and 52.06 – 69.33 mM (red dots). (b) Plot of  $k_{obs}$  vs. [TFA], 4.35 – 43.41 mM (blue dots) and 52.06 – 69.33 mM (red dots). (c) Plot of logarithm of  $k_{obs}$  vs. logarithm of [TFA] within the same concentration range as used in (a) and (b). The  $R^2$  values for all linear fits are  $> 0.97$ .

The catalytic rate constants ( $k_{obs}$ ) at different TFA concentrations were extracted considering the catalytic peak currents with higher current densities at potentials near to the reduction potential of  $Ni^{II}/Ni^0$  and using Eq. 1,<sup>12</sup> where  $k_1$  is the second-order rate constant for the first protonation step,  $i_{cat}/i_p$  denotes the ratio of the catalytic peak current to the noncatalytic peak current of the  $Ni^{II}/Ni^0$  reduction, and  $v$  is the scan rate (0.1 V/s).

$$k_{obs} = k_1 \times [TFA]^x = 1.94 \text{ V}^{-1} \times v \times (i_{cat}/i_p)^2; \quad \text{Eq. 1}$$

The  $k_{\text{obs}}$  values showed a linear regression with the TFA concentrations of  $\leq 0.043$  M (Figure 5b, blue dots). A linear fit yielded the slope value, which implies the second-order rate constant,  $k_1$  of  $1.53 \times 10^4 \text{ M}^{-1} \text{ s}^{-1}$ . Interestingly, such linear correlation showed a much steeper slope at TFA concentrations higher than 0.043 M (Figure 5b, red dots). This also supports a change in the HER mechanism of  $1^{2+}$  at higher proton concentration.<sup>14</sup> Furthermore, the linear fits of the logarithm of  $k_{\text{obs}}$  vs. the logarithm of [TFA], either at concentrations lower and higher than 0.043 M, provide slopes of 1.56 and 2.2, respectively (Figure 5c). Overall, these slope values suggest a reaction order of  $\sim 2$  with respect to the TFA concentration in the rate-limiting step.

Based on these electrochemical results, we propose an overall catalytic HER cycle in which  $1^{2+}$  is converted into **1** via a single  $2e^-$  reduction step, followed by a proton transfer event at low acid concentrations (Figure 6). The reaction order in acid concentration suggests the involvement of 2 molecules of TFA in the rate-limiting step, yet it contradicts the change in  $E_{\text{Ni(II/I)}}$  of 23 mV/dec, since two consecutive steps with an equal number of electrons and protons should yield a Nernstian slope of 59 mV/dec.<sup>20</sup> Therefore, we attribute the participation of 2 molecules of TFA in the rate-limiting protonation step leading to the formation of a Ni<sup>II</sup>-hydride species **2**, in which a pyridyl group of the N2S2 ligand forms a H-bond with a TFA molecule. Subsequently, **2** becomes **3** upon protonation of the non-coordinating pyridyl group of N2S2, which then releases H<sub>2</sub> and returns to the resting state,  $1^{2+}$ . In contrast, in the presence of TFA in concentrations higher than 0.043 M, a change in the HER mechanism is proposed (Figures 5a and 5b). We interpret that the shift in  $E_{\text{Ni(II/I)}}$  with a slope of 179 mV/dec at higher H<sup>+</sup> concentrations is due to a CPET process involving  $2\text{H}^+$  and  $1e^-$  in the rate-limiting step (Figure 6, orange pathway).<sup>20-21</sup> Thus, both pathways (Figure 6, blue and orange arrows) lead to complex **3**, where one pyridyl group of the N2S2 ligand is protonated and thus mimics the Cys residue in the Ni-R state of [NiFe] hydrogenase, and also by shuttling between a metal-bound state and a protonated state during the HER catalytic cycle.

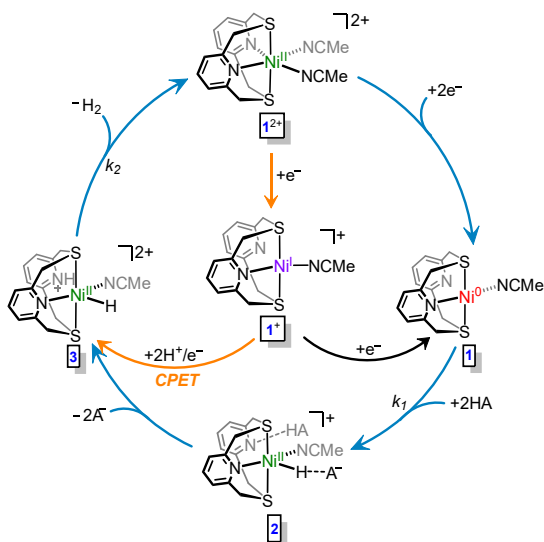


**Figure 6.** Proposed catalytic HER cycle for  $1^{2+}$  at low ( $\leq 0.043$  M, blue) and high (orange) TFA concentrations. The final step (**3** to  $1^{2+}$ ) is common for both pathways. The black arrow indicates the redox step in the absence of an acid. HA = TFA, CPET = Concerted proton-coupled electron transfer.

We also performed electron paramagnetic resonance (EPR) spectroscopy to detect a Ni<sup>I</sup> species upon reducing  $1^{2+}$  with 1 equiv of  $\text{CoCp}^*_2$  ( $\text{Cp}^*$  = pentamethylcyclopentadienyl). The X-band EPR spectrum in 1:3 MeCN:PrCN (v/v) at 77 K exhibited an EPR signal that was simulated using a rhombic g tensor ( $g_x = 2.205$ ,  $g_y = 2.152$ ,  $g_z = 2.012$ ). We attribute this EPR signal to a  $(\text{N}_2\text{S}_2)\text{Ni}^{\text{I}}$  species such as  $1^+$ , suggesting a  $d_{x^2-y^2}$  ground state in a square planar geometry, and based also on the comparison with the EPR spectra of other reported Ni<sup>I</sup> complexes.<sup>22-23</sup>

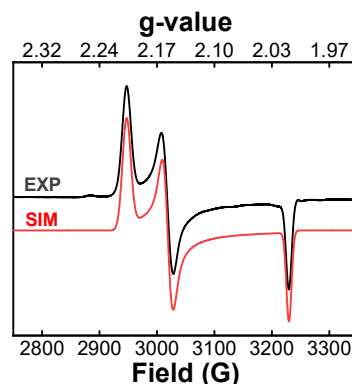


**Figure 7.** Experimental (black) and simulated (red) EPR spectra for  $1^{2+}$  after treating it with 1 equiv. of  $\text{CoCp}^*_2$  in 1:3 MeCN:PrCN glass at 77 K. The following g values were used for the simulation:  $g_x = 2.205$ ,  $g_y = 2.152$ ,  $g_z = 2.012$ .

It is important to note that strong acids are known to undergo a homoconjugation process in organic solvents. The addition of H<sub>2</sub>O is a commonly used additive to impede such homoconjugation events and hence enhance the HER kinetics, without interfering with the thermodynamic parameters.<sup>17</sup> To evaluate the effect of H<sub>2</sub>O on HER catalysis, we limited the concentration of TFA up to 0.043 M in MeCN and added three different H<sub>2</sub>O concentrations, 1.0, 1.5, and 2.0 M. Linear sweep voltammograms (LSVs) recorded for  $1^{2+}$  under these conditions showed plateau currents at potentials lower than  $-1.75$  V, and the shape of the LSVs remained unchanged as more H<sub>2</sub>O was added (Figure 8).

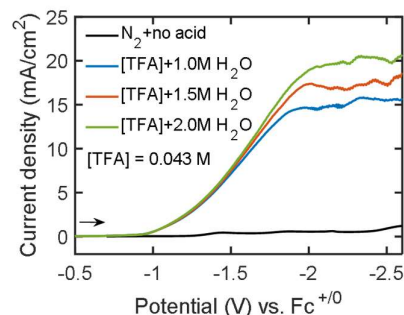


**Figure 8.** Linear sweep voltammograms for  $1^{2+}$  recorded in N<sub>2</sub>-saturated 0.1 M TBAP/MeCN in the absence of TFA (blue) and the presence of 0.043 M TFA + different concentration of H<sub>2</sub>O, 1 M (orange), 1.5 M (yellow), and 2.0 M (purple). Scan rate = 0.1 V/s. The uneven features at the plateau-current regions could be due to the formation of H<sub>2</sub> bubbles at the surface of the electrode.

Foot-of-the-wave analysis (FOWA) was then carried out and the maximum TOFs at three different H<sub>2</sub>O concentrations in MeCN with 0.043 M of TFA were estimated (Figure 9a and Table S1).<sup>19</sup> The average  $\text{TOF}_{\text{max}}$  observed for  $1^{2+}$  is  $1.95 \times 10^5 \text{ s}^{-1}$ . It is

noteworthy that the  $\text{TOF}_{\text{max}}$  values are independent of the  $\text{H}_2\text{O}$  concentration (Figure 9b), and thus the role of  $\text{H}_2\text{O}$  herein can be described as mainly impeding the homoconjugation process of TFA in MeCN.<sup>17</sup> Although such inhibition of the homoconjugation process should increase the availability of more  $\text{H}^+$  from TFA, the negligible effect on  $\text{TOF}_{\text{max}}$  upon the addition of  $\text{H}_2\text{O}$  also highlights the role of the pendant pyridinium ion in complex **3** toward HER. Overall, we posit that complex **3** can produce  $\text{H}_2$  as long as the pyridyl group of the N2S2 ligand is protonated, no matter how acidic the bulk electrolyte is.

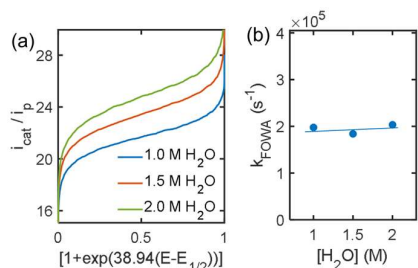


**Figure 9.** (a) FOWA for  $1^{2+}$  in  $\text{N}_2$ -saturated 0.1 M TBAP/MeCN + 0.043 M TFA at different concentration of  $\text{H}_2\text{O}$ ; 1 M (blue), 1.5 M (orange), and 2 M (yellow). The most linear portion at the lower range of  $1/1+\exp(38.94(E-E_{1/2}))$  values are fitted linearly to extract the rate constant ( $k_{\text{FOWA}}$ ,  $\text{s}^{-1}$ ).<sup>19</sup> (b) The  $k_{\text{FOWA}} = \text{TOF}_{\text{max}}$  values obtained from (a) are plotted vs. the concentration of  $\text{H}_2\text{O}$ .

The overpotential for the HER process was then calculated using the Appel and Helm method,<sup>24</sup> and was found to be 730 mV at  $E_{\text{cat}/2}$  for  $1^{2+}$  in the presence of 0.043 M TFA with 1.5 M  $\text{H}_2\text{O}$  in MeCN. Under such acidic MeCN conditions, chronoamperometric experiments carried out for  $1^{2+}$  showed a total charge of 200 mC passed over 15 mins of electrolysis at an applied potential of  $E_{\text{cat}/2}$ , which correspond to the accumulation of  $1.03 \times 10^{-6}$  moles of  $\text{H}_2$  (Figure S13).  $\text{H}_2$  was detected by transferring the headspace of the post-electrolysis solution and using gas chromatography. It is noteworthy that the current efficiency was greater than ~98%, and the average currents were much higher than the background contribution (Figure S13).

To benchmark the HER activity of  $1^{2+}$ , we selected five efficient Ni<sup>II</sup>-based HER electrocatalysts, **4**,<sup>15</sup> **5**<sup>2+</sup>,<sup>16</sup> **6**<sup>2+</sup>,<sup>12</sup> **7**<sup>2+</sup>,<sup>13</sup> and **8**<sup>2+</sup> (Figure 10a).<sup>14</sup> We have included the reported TOF values for these electrocatalysts and calculated the overpotentials by correcting the standard thermodynamic potentials ( $E_{\text{HA}}$ ) for  $\text{H}^+$ -to- $\text{H}_2$  conversion at the given  $\text{pK}_a$  of the acid (HA) used in the corresponding non-aqueous electrolyte (Eq. 2).<sup>17</sup>

$$E_{\text{HA}} = E^0 - (2.303RT/F) \times \text{pK}_a(\text{HA}); \quad \text{Eq. 2}$$

In Eq. 2,  $E^0$  is  $-0.028 \text{ V vs. Fc}^{+/0}$  and  $RT/F$  is calculated as 0.026 V.<sup>17</sup> The logarithm of the TOFs were then plotted vs. the calculated overpotentials ( $E^0 - E_{\text{HA}}$ ) for the reported Ni complexes mentioned above and  $1^{2+}$  (Figure 10b). Remarkably, our  $1^{2+}$  complex performs electrocatalytic HER at a much higher TOF than that of **4**, **5**<sup>2+</sup>, **6**<sup>2+</sup>, and **7**<sup>2+</sup> (the reported acid concentration for these complexes is given in the Figure 10 caption). On the contrary, the overpotential for  $1^{2+}$  is higher than most of these reported Ni complexes, yet is comparable with that for **6**<sup>2+</sup>, albeit **6**<sup>2+</sup> employs a strong acid,  $[(\text{DMF})\text{H}]^+$ , at concentrations  $>0.4 \text{ M}$ . Although  $1^{2+}$  is somewhat inferior to **8**<sup>2+</sup> in terms of energetics, it is important to note that **8**<sup>2+</sup> requires the use of  $\leq 0.6 \text{ M}$  anilinium ( $\text{pK}_a = 10.62$  in MeCN)<sup>14, 17</sup> that implies a stronger acid strength than  $\leq 0.043 \text{ M}$  of TFA in MeCN. Overall, the electrochemical

HER performance of  $1^{2+}$  is significant, especially since competitive HER kinetics can be achieved at low acid concentrations using a weaker acid. By comparison, the only other Ni HER electrocatalysts containing thiolate and/or pyridine ligands, **4** and **5**<sup>2+</sup>, exhibit TOFs that are at least two orders of magnitude lower than that of  $1^{2+}$ .

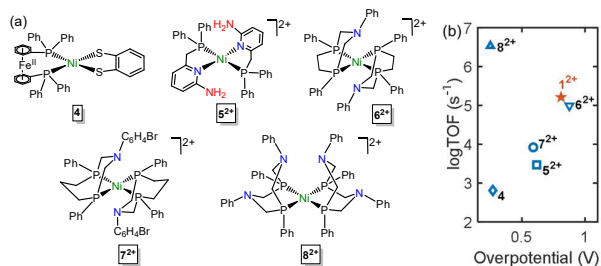


**Figure 10.** (a) Selected Ni<sup>II</sup> HER electrocatalysts reported for efficient HER: **4**,<sup>15</sup> **5**<sup>2+</sup>,<sup>16</sup> **6**<sup>2+</sup>,<sup>12</sup> **7**<sup>2+</sup>,<sup>13</sup> and **8**<sup>2+</sup>.<sup>14</sup> The proton sources used are: 0.05 M AcOH in THF for **4**, 0.3 M AcOH in MeCN for **5**<sup>2+</sup>, 0.42 M  $[(\text{DMF})\text{H}]^+ + 1.2 \text{ M H}_2\text{O}$  in MeCN for **6**<sup>2+</sup>, 1.26 M  $[(\text{DMF})\text{H}]^+ + 1.09 \text{ M H}_2\text{O}$  in MeCN for **7**<sup>2+</sup>, and 0.6 M anilinium in MeCN for **8**<sup>2+</sup>. (b) Comparison of the logarithm of TOF vs. the calculated overpotential reported for the Ni electrocatalysts shown in (a) and  $1^{2+}$ , the latter being in the presence of 0.043 M TFA + 1.5 M  $\text{H}_2\text{O}$  in MeCN.

In summary, we have synthesized and characterized a bioinspired  $[(\text{N}2\text{S}2)\text{Ni}(\text{MeCN})_2]^{2+}$ ,  $1^{2+}$ , complex that is an efficient HER electrocatalyst. This complex catalytically reduces protons to  $\text{H}_2$  at very low acid (TFA) concentrations. Given that most of the reported Ni-based molecular HER electrocatalysts perform HER using stronger acids than TFA, and often at high acid concentrations,<sup>12-14</sup> the performance of  $1^{2+}$  is remarkable as it achieves a very high TOF at low acid concentrations. In addition, we highlight the role of the pendant pyridyl group of the N2S2 ligand in leading to elevated HER kinetics, which we consider it resembles the proton-relay role of the Cys residue in  $[\text{NiFe}]$  hydrogenases that shuttles between a metal-bound and a protonated state. Although  $1^{2+}$  catalyses the HER process at a high overpotential, 0.7 V, its proposed HER mechanism should inspire the development of biomimetic HER electrocatalysts that operate under benign reaction conditions.

## Acknowledgements

We thank the Department of Energy's BES Catalysis Science Program (DE-SC0006862) for financial support of the initial studies. We thank Prof. Nigam P. Rath (Univ. of Missouri - St. Louis) for obtaining the crystal structure of **1**•(OTf)<sub>2</sub>. We also thank all the research facilities in the Department of Chemistry at the University of Illinois at Urbana-Champaign for their help.

**Keywords:** electrocatalysis • hydrogen evolution reaction • bioinspired catalysts • Ni complexes •  $[\text{NiFe}]$  hydrogenase

## References

- Lewis, N. S.; Nocera, D. G., Powering the planet: Chemical challenges in solar energy utilization. *Proc. Nat. Acad. Sci. USA* **2006**, *103* (43), 15729-15735.
- Jones, A. K.; Sillery, E.; Albracht, S. P.; Armstrong, F. A., Direct comparison of the electrocatalytic oxidation of hydrogen by an

- enzyme and a platinum catalyst. *Chem. Commun.* **2002**, (8), 866-7.
3. Madden, C.; Vaughn, M. D.; Díez-Pérez, I.; Brown, K. A.; King, P. W.; Gust, D.; Moore, A. L.; Moore, T. A., Catalytic Turnover of [FeFe]-Hydrogenase Based on Single-Molecule Imaging. *J. Am. Chem. Soc.* **2012**, *134* (3), 1577-1582.
  4. Armstrong, F. A., Hydrogenases: active site puzzles and progress. *Curr. Opin. Chem. Biol.* **2004**, *8* (2), 133-140.
  5. De Lacey, A. L.; Fernandez, V. M.; Rousset, M.; Cammack, R., Activation and inactivation of hydrogenase function and the catalytic cycle: spectroelectrochemical studies. *Chem. Rev.* **2007**, *107* (10), 4304-30.
  6. Lubitz, W.; Ogata, H.; Rüdiger, O.; Reijerse, E., Hydrogenases. *Chem. Rev.* **2014**, *114* (8), 4081-4148.
  7. Perra, A.; Davies, E. S.; Hyde, J. R.; Wang, Q.; McMaster, J.; Schröder, M., Electrocatalytic production of hydrogen by a synthetic model of [NiFe] hydrogenases. *Chem. Comm.* **2006**, (10), 1103-1105.
  8. Tanino, S.; Li, Z.; Ohki, Y.; Tatsumi, K., A Dithiolate-Bridged (CN)<sub>2</sub>(CO)Fe-Ni Complex Reproducing the IR Bands of [NiFe] Hydrogenase. *Inorg. Chem.* **2009**, *48* (6), 2358-2360.
  9. Ohki, Y.; Yasumura, K.; Kuge, K.; Tanino, S.; Ando, M.; Li, Z.; Tatsumi, K., Thiolate-bridged dinuclear iron(tris-carbonyl)-nickel complexes relevant to the active site of [NiFe] hydrogenase. *Proc. Natl. Acad. Sci. U. S. A.* **2008**, *105* (22), 7652.
  10. Barton, B. E.; Whaley, C. M.; Rauchfuss, T. B.; Gray, D. L., Nickel-iron dithiolato hydrides relevant to the [NiFe]-hydrogenase active site. *J. Am. Chem. Soc.* **2009**, *131* (20), 6942-3.
  11. Canaguier, S.; Field, M.; Oudart, Y.; Pécaut, J.; Fontecave, M.; Artero, V., A structural and functional mimic of the active site of NiFe hydrogenases. *Chem. Comm.* **2010**, *46* (32), 5876-5878.
  12. Helm, M. L.; Stewart, M. P.; Bullock, R. M.; DuBois, M. R.; DuBois, D. L., A Synthetic Nickel Electrocatalyst with a Turnover Frequency Above 100,000 s<sup>-1</sup> for H<sub>2</sub> Production. *Science* **2011**, *333* (6044), 863-866.
  13. Wiese, S.; Kilgore, U. J.; Ho, M.-H.; Raugei, S.; DuBois, D. L.; Bullock, R. M.; Helm, M. L., Hydrogen Production Using Nickel Electrocatalysts with Pendant Amines: Ligand Effects on Rates and Overpotentials. *ACS Catal.* **2013**, *3* (11), 2527-2535.
  14. Rountree, E. S.; Dempsey, J. L., Potential-Dependent Electrocatalytic Pathways: Controlling Reactivity with pK(a) for Mechanistic Investigation of a Nickel-Based Hydrogen Evolution Catalyst. *J. Am. Chem. Soc.* **2015**, *137* (41), 13371-13380.
  15. Gan, L.; Groy, T. L.; Tarakeshwar, P.; Mazinani, S. K.; Shearer, J.; Mujica, V.; Jones, A. K., A nickel phosphine complex as a fast and efficient hydrogen production catalyst. *J. Am. Chem. Soc.* **2015**, *137* (3), 1109-15.
  16. Tatematsu, R.; Inomata, T.; Ozawa, T.; Masuda, H., Electrocatalytic Hydrogen Production by a Nickel(II) Complex with a Phosphinopyridyl Ligand. *Angew. Chem., Int. Ed.* **2016**, *55* (17), 5247-5250.
  17. McCarthy, B. D.; Martin, D. J.; Rountree, E. S.; Ullman, A. C.; Dempsey, J. L., Electrochemical Reduction of Brønsted Acids by Glassy Carbon in Acetonitrile—Implications for Electrocatalytic Hydrogen Evolution. *Inorg. Chem.* **2014**, *53* (16), 8350-8361.
  18. Moriguchi, T.; Kitamura, S.; Sakata, K.; Tsuge, A., Syntheses and Structures of Dichloropalladium(II)(Dithia[3.3]Metadipyridinophane) and Dichloroplatinum(II)(Dithia[3.3]Metadipyridinophane) Complexes. *Polyhedron* **2001**, *20* (18), 2315-2320.
  19. LiviuNote2020, See Supporting Information.
  20. Bard, A. J.; Faulkner, L. R., *Electrochemical methods: Fundamentals and applications*. Wiley: 2001.
  21. Jackson, M. N.; Kaminsky, C. J.; Oh, S.; Melville, J. F.; Surendranath, Y., Graphite Conjugation Eliminates Redox Intermediates in Molecular Electrocatalysis. *J. Am. Chem. Soc.* **2019**, *141* (36), 14160-14167.
  22. Becker, J. Y.; Kerr, J. B.; Pletcher, D.; Rosas, R., The electrochemistry of square planar macrocyclic nickel complexes and the reaction of Ni(I) with alkyl bromides: Nickel tetraamine complexes. *J. Electroanal. Chem. Interf. Electrochem.* **1981**, *117* (1), 87-99.
  23. Mohadjer Beromi, M.; Brudvig, G. W.; Hazari, N.; Lant, H. M. C.; Mercado, B. Q., Synthesis and Reactivity of Paramagnetic Nickel Polypyridyl Complexes Relevant to C(sp<sup>2</sup>)-C(sp<sup>3</sup>) Coupling Reactions. *Angew. Chem., Int. Ed.* **2019**, *58* (18), 6094-6098.
  24. Appel, A. M.; Helm, M. L., Determining the Overpotential for a Molecular Electrocatalyst. *ACS Catal.* **2014**, *4* (2), 630-633.

